PHYSICAL REVIEW B **79**, 075308 (2009)

Negative differential conductivity of two-dimensional electron-gas systems in high magnetic fields

J. C. Chen, Yuling Tsai, and Yiping Lin
Department of Physics, National Tsing-Hua University, 101, Section 2, Kuang-Fu Road, Hsinchu, Taiwan 30013, Republic of China

T. Ueda and S. Komiyama
Department of Basic Science, University of Tokyo, Komaba 3-8-1, Meguro-ku, Tokyo 153-8902, Japan
(Received 27 October 2008; published 10 February 2009)

Nonlinear effects of two-dimensional electron-gas systems at high magnetic fields are studied, and a current-driven instability is found to take place in magnetic fields corresponding to integer filling factors of Landau levels. The current instability is ascribed to the occurrence of a negative differential conductivity, predicted theoretically more than three decades ago. Physical origin of the negative differential conductivity is discussed and suggested to originate from an electric-field-induced reduction in the average scattering probability of electrons.

DOI: 10.1103/PhysRevB.79.075308 PACS number(s): 73.43.Qt, 71.70.Di

I. INTRODUCTION

Instability associated with negative differential conductivity (NDC) in two-dimensional electron-gas (2DEG) systems has attracted much research interest recently. To a large extent studies have been stimulated by the recent finding of "zero-resistance state" in high-mobility 2DEG systems in GaAs/AlGaAs heterostructure crystals under strong microwave radiation.[1–3] It is theoretically suggested that the conductivity σ_{xx} may become negative in the presence of the radiation and a magnetic field.[4–8] Understanding of the origin of the NDC may be crucial for clarifying the possible mechanism behind the phenomenon.

In the absence of magnetic fields, NDC in bulk semiconductors has been extensively studied for nearly four decades.[9] The NDC is characterized by a multivalued dependence in the current-voltage (I-V) relationship, viz., V is a multivalued function of I when the I-V curve is N shaped, while I is a multivalued function of V when the I-V curve is S shaped. In either case, the electron system becomes unstable against fluctuation of the space-charge distribution. A steady state may be reached if a particular mode of space-charge distribution exponentially grows, but otherwise, the system may continue to fluctuate without reaching steady state. It is well known that the N-shaped NDC develops high-electric field domains while the S-shaped NDC leads to formation of high-current filaments.

Although NDC in the presence of magnetic fields has not been studied so extensively as the one in the absence of magnetic field,[10] it is more than three decades ago when Kurosawa *et al.*[11] provided generalized discussion of NDC in arbitrary magnetic fields. It was shown theoretically that NDC is made more probable as the Hall angle ψ approaches $\pi/2$ in strong magnetic fields. Let J be a current flowing in dc electric field E in the presence of a magnetic field B perpendicular to E. A small variation, ΔE, in E causes a response, ΔJ, in J as illustrated in Fig. 1(a). Kurosawa *et al.*[11] noted that the generalized condition of NDC is that the inequality relation

$$\Delta J \cdot \Delta E < 0 \tag{1}$$

holds in some direction of ΔE. If ΔE is induced by a sheet of space charge shown in Fig. 1(b), the response current ΔJ satisfying relation (1) increases the original space charge. Thus the space-charge sheet exponentially grows up, making the system unstable. In strong magnetic fields, the angle between ΔE and ΔJ is close to $\pi/2$ even if the J-E relation is strictly linear. As will be explicitly described later, the angle can exceed $\pi/2$ with infinitesimal nonlinearities as ψ approaches $\pi/2$.

The quantum-Hall (QH) electron system is an interesting candidate for studying such NDC because ψ is nearly equal to $\pi/2$. Although experiments have demonstrated that the QH effect state is a stable state without exhibiting NDC at low E and low lattice temperatures T_L, NDC may occur at higher values of E and elevated T_L, where significant nonlinearity in the current response can be expected. Experimental observation of this type of NDC was briefly reported two decades ago.[12] The mechanism behind the NDC, however, was left unclear.

The negative conductivity states discussed in Refs. 4–8 are the NDC induced by intense alternating electric fields in the presence of weak dc fields. The symmetry point of the N- or S-shaped I-V curve is shifted to the origin of the coordinates under microwave illumination.[6] Based on these new

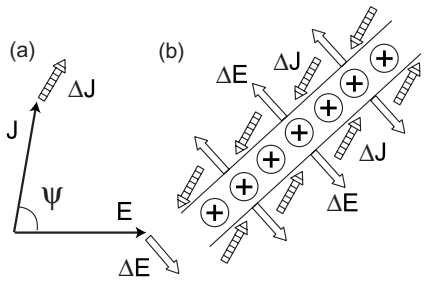

FIG. 1. (a) A sketch of $\Delta J \cdot \Delta E < 0$, where $J \cdot E > 0$ under strong magnetic fields. (b) Growth of a space-charge sheet in the condition of $\Delta J \cdot \Delta E < 0$. (Adopted from Fig. 1 in Ref. 11.)

theoretical developments, few experiments have attempted to study these nonlinear phenomena in nonequilibrium 2DEG systems at high magnetic field.[13–16] Although those phenomena may bear little direct relevance to the NDC discussed here, understanding of the NDC in strong dc electric fields may provide a firm and sound platform for exploring the nature of the alternating-field-induced NDC.

Here we study transport properties of 2DEG systems in $GaAs/Al_xGa_{1-x}As$ heterostructures up to high-current levels in high magnetic fields. We find that current instability takes place due to the NDC predicted theoretically more than three decades ago.[11] This paper is organized as follows. Section II describes device geometry and experimental method along with experimental results including the observation of current instability. In Sec. III A, nonlinear response of the system is clarified by deriving differential transport coefficients, and the current instability is ascribed to the occurrence of the NDC discussed in Ref. 11. In Sec. III B, a particular profile of the space-charge needle (filament) is suggested to grow in the regime of the NDC. Low-temperature characteristics are discussed in Sec. III C. In Sec. III D, physical mechanism leading to the nonlinear transport coefficients is discussed. In Sec. IV, we conclude that NDC is a general feature of high-mobility 2DEG systems in high magnetic fields when the Landau-level (LL) filling factor is close to an integer.

II. EXPERIMENTAL METHODS AND RESULTS

Samples have been prepared in two different modulation-doped $GaAs/Al_{0.3}Ga_{0.7}As$ single heterostructure crystals grown by molecular-beam epitaxy. Sample 1 is a 100-μm-wide Hall bar with two pairs of voltage probes placed at a distance of 200 μm as schematically shown in the inset of Fig. 2(a). The device is fabricated in a wafer of an electron density of $N_s=3.1\times10^{11}$ cm^{-2} and a 4.2 K mobility of $\mu=8.0\times10^5$ cm^2/Vs. Sample 2 is similar to the one described in Ref. 12, which is a 50-μm-wide Hall bar with three pairs of voltage probes separated at a 100 μm distance. The device is fabricated in a wafer of $N_s=3.8\times10^{11}$ cm^{-2} and $\mu=4.0\times10^5$ cm^2/Vs. Similar experimental results have been obtained in samples 1 and 2. For the reason of space, however, experimental results of sample 1 will be mainly described below. Most of the measurements are carried out by transmitting square-wave current (17 Hz) alternating between $I=0$ and $I=I_{SD}$ through contacts 5 and 6, $I_{SD}=I_{56}$. The longitudinal voltage, V_{xx}, is studied by recording the voltage difference between contacts 1 and 2 (V_{12}) or contacts 3 and 4 (V_{34}), and the Hall voltage, V_{xy}, by V_{13} or V_{24}. At elevated temperatures ($T_L>7$ K for $\nu=4$ and $T_L>13$ K for $\nu=2$), the values of V_{xx} and V_{xy} obtained with different pairs of voltage probes were found to agree with one another within an accuracy of 10^{-3}, which allow us to assume that the spatial distribution of the current or the electric field should be highly uniform.

Figure 2(a) displays the curves of $R_{xx}=V_{12}/I_{SD}$ and $R_{xy}=V_{13}/I_{SD}$ versus B in sample 1 taken at $T=4.2$ K with $I_{SD}=0.1$ μA. As will be described below, nonlinear response of the system at higher levels of I_{SD} is similar between the filling factors of $\nu=2$ ($B=5.88$ T) and $\nu=4$ ($B=2.94$ T).

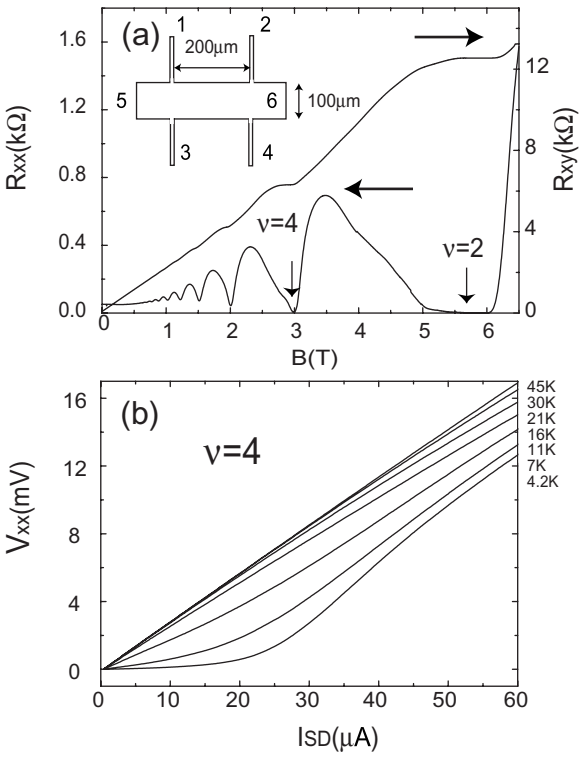

FIG. 2. (a) Longitudinal resistance R_{xx} and Hall resistance R_{xy} at 4.2 K and $I_{SD}=0.1$ μA in sample 1. The inset is a schematic of the device geometry. (b) Dependence of the voltage along the channel V_{xx} on the source-drain current I_{SD} at $\nu=4$ with the temperature as a parameter.

The current instability, however, shows up only at $\nu=2$.

Figure 2(b) shows the dependence of $V_{xx}=V_{12}$ on I_{SD} at $\nu=4$ for different temperatures. At 4.2 K, V_{xx} increases abruptly when I_{SD} exceeds ~20 μA, which is ascribed to the current-induced breakdown of the integer Quantum Hall effect (IQHE).[17,18] At elevated temperatures, V_{xx} is already finite in the limit of small I_{SD}. We note that the curves of V_{xx} versus I_{SD} are smooth, which are free from any anomalous structures. Closer look at the data ($T_L>16$ K) clarifies that the increase in V_{xx} is weakly sublinear. Though not shown here, the increase in V_{xy} with increasing I_{SD} at elevated temperatures is slightly superlinear.

The dependence of V_{xx} on I_{SD} at $\nu=2$ is shown in Fig. 3(a). Overall features are similar to those of the data at $\nu=4$. At lower temperatures ($T_L<10$ K), V_{xx} rapidly increases with increasing I_{SD} above a certain critical value due to the current-induced breakdown. At elevated temperatures ($16\le T_L\le28$ K), V_{xx} increases sublinearly with increasing I_{SD}, similar to the case of $\nu=4$. Differently from the data at $\nu=4$, however, the smooth sublinear increase is terminated by a kink ($I_{SD}=I_{th}$), above which V_{xx} abruptly drops and the voltage starts to significantly fluctuate. The threshold current, I_{th}, increases with increasing the lattice temperature T_L as marked by the arrows in Fig. 3(a). For later analysis, the electric field values reached at I_{th}, derived from $E_{th}=[(V_{xx}/L)^2+(V_{xy}/W)^2]^{1/2}$ with the inter-voltage probe distance $L=200$ μm and the Hall-bar width $W=100$ μm for sample 1, are listed on Table I along with the values of I_{th}.

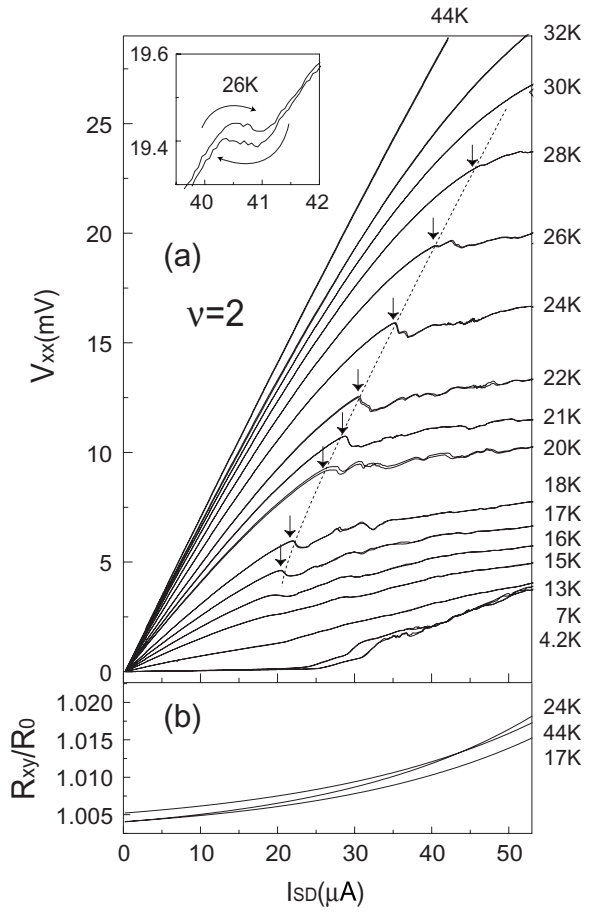

FIG. 3. (a) V_{xx} vs I_{SD} for $\nu=2$ Hall plateau in sample 1. The arrows mark the threshold current $I_{\mathrm{DS}}=I_{\mathrm{th}}$, above which the current instability takes place. The inset shows an example of zigzaglike dependence and hysteresis in V_{xx}-I_{SD} curve above I_{th} at $T_L=26$ K. (b) The Hall resistance R_{xy} as a function of I_{SD}, where values of R_{xy} are normalized by the value at zero current limit, $R_0=V_H/I_{\mathrm{SD}}|_{I_{\mathrm{SD}}=0}$. Note that the cyclotron energy is $\hbar\omega_c/k_B\approx 118$ K at $\nu=2$ ($B=5.88$ T), where $\hbar\omega_c$ is the cyclotron energy and k_B is the Boltzmann constant.

The fluctuation of V_{xx} is visible as small irregular structures in the V_{xx} versus I_{DS} curves in Fig. 3(a). Some of the structures are reproducible but the others are random fluctuations. The curves also exhibit hysteresis when the direction of current scan is reversed as the example shown in the inset of Fig. 3(a).

The increase in V_{xy} with increasing I_{SD} ($T_L>15$ K) is found to be slightly superlinear. It follows that the Hall resistance $R_{xy}=V_{xy}/I_{\mathrm{SD}}$ increases slightly with increasing I_{SD} as shown in Fig. 3(b), where R_{xy} is normalized by its value, R_0, at small I_{SD} and $T_L=4.2$ K. Curves at three different temperatures are displayed in Fig. 3(b), where the curves at other elevated temperatures ($T_L>15$ K) are all similar to each other.

As already mentioned, the values of V_{xx} and V_{xy} in the stable region ($I_{\mathrm{SD}}\leq I_{\mathrm{th}}$ and $T_L>15$ K) are substantially independent of the voltage probes used, viz., values of V_{12} and V_{34} and those of V_{13} and V_{24} agree with one another to an accuracy better than 10^{-3}. In the unstable region, $I_{\mathrm{SD}}>I_{\mathrm{th}}$, the values of V_{12} and V_{34} differ appreciably although the overall feature of the V_{xx} versus I_{SD} curves is similar. We have also confirmed that the effects described above (and below) are independent of the polarity of current and magnetic field.

In sample 2, we carried out similar measurements both at $\nu=4$ and $\nu=2$, and obtained similar experimental results described above for sample 1, viz., V_{xx} is found to sublinearly increase with I_{SD} both at $\nu=4$ and $\nu=2$ but current instability shows up only at $\nu=2$. The curves of V_{xx} versus I_{SD} are featured with similar structures to those shown in Fig. 3(a). No instability is seen at $\nu=4$.

The experimental results (Figs. 2 and 3) for $I_{\mathrm{SD}}<I_{\mathrm{th}}$ are found to be substantially independent of the choice of voltage probes; thus we assume that the distribution of the electric field E or the current density J is highly uniform in the Hall bars at elevated temperatures in our following analysis. These features, along with the fact that the phenomena are independent of the polarities of current and magnetic field, suggest strongly that (i) the current instability found here is intrinsic to the 2DEG system at high magnetic fields and (ii) the effect is controlled by the local conductivity tensor. We should mention, however, that the current instability takes place only at $\nu\sim 2$, although the sublinear dependence of V_{xx} on I_{SD} is similar between $\nu\sim 2$ and $\nu\sim 4$.

III. DISCUSSION

A. Condition of NDC

Generalized condition of NDC is that inequality (1) is satisfied in some direction of ΔE. Kurosawa *et al.*[11] described this criterion in terms of differential conductivity tensor, σ^d, defined by $\Delta J_i=\Sigma_j(\partial J_i/\partial E_j)\Delta E_j=\Sigma_j\sigma^d_{ij}\Delta E_j$. The tensor is decomposed into a symmetric and an antisymmetric parts: $\sigma^d=\sigma^d_S+\sigma^d_A$. The criterion of the NDC is equivalent such that the symmetric matrix, σ^d_S, is of a negative eigenvalue. This requirement, in turn, is equivalent to the condition that σ^d_S is of a negative determinant, which is explicitly represented by the inequality

$$D=\beta^2\tan^2\psi+2\alpha(2-\beta)\tan\psi+\alpha^2-4(1-\beta)>0, \quad (2)$$

where $\alpha=\partial\psi/\partial\log E=E(\partial\psi/\partial E)$ is the nonlinear parameter characterizing the change in the Hall angle ψ and $\beta=1$

TABLE I. Values of I_{th}, E_{th}, and E_{NDC} for each T_L derived from the data in Figs. 3(a), 3(b), and 4(e).

T_L	(K)	17	20	22	24	26	28
I_{th}	(μA)	20.3 ± 0.4	27.3 ± 0.7	30.4 ± 0.3	35.1 ± 0.4	40.9 ± 0.7	46.9 ± 0.4
E_{th}	(V/cm)	26.1 ± 0.5	35.1 ± 0.7	39.1 ± 0.4	45.2 ± 0.4	51.7 ± 0.9	60.7 ± 0.5
E_{NDC}	(V/cm)	25.8 ± 0.4	35.1 ± 0.3	38.9 ± 0.3	45.0 ± 0.3	52.8 ± 0.4	61.1 ± 0.3

$-(\partial \log J/\partial \log E)=1-(E/J)(\partial J/\partial E)$ is the parameter characterizing the nonlinear increase in the current J. If the response is strictly linear, $\alpha=\beta=0$ and $D=-4$. In the presence of nonlinearity ($\alpha\neq 0$ and/or $\beta\neq 0$), D can be larger than -4, eventually reaching positive values. In the absence of magnetic field ($\alpha=0$), relation (2) is reduced to the familiar condition of NDC, $\beta>1$ or $\partial J/\partial E<0$. We note in relation (2) that the NDC becomes more and more probable as $\tan\psi \gg 1$ increases. [This will be made explicit in relation (3).]

Since in the experiments E and J are assumed to be highly uniform at elevated temperatures, we can evaluate α, β, and ψ up to $I_{SD}=I_{th}$ from the experimental data of V_{xx} and V_{xy} ($T_L>13$ K). We first derive values of E, J, and ψ as a function of I_{SD} through the relations $E=[(V_{xx}/L)^2+(V_{xy}/W)^2]^{1/2}$, $J=I_{SD}/W$, and $\psi=\tan^{-1}(V_{xy}L/V_{xx}W)$, where $L=200$ μm and $W=100$ μm for sample 1 and $L=100$ μm and $W=50$ μm for sample 2.

Values of $\psi(E)$ and $J(E)$ are shown as a function E in Figs. 4(a) and 4(b) for sample 1 ($\nu=2$) at several elevated temperatures. The amplitude of ψ [Fig. 4(a)] increases with increasing E because of the sublinear increase in V_{xx} with I_{SD} [Fig. 3(a)]. Figure 4(b) displays J-E curve at $T_L=20$ K. The other curves at elevated temperatures ($16\leq T_L\leq 44$ K) are similar to the curve of 20 K. Though not clear in Fig. 4(b), J depends sublinearly on E because of the superlinear increase in V_{xy} with increasing I_{SD} [Fig. 3(b)].

Parameters α and β are numerically derived from the data of $\psi(E)$ and $J(E)$ up to $E=E_{th}$ and are shown, respectively, in Figs. 4(c) and 4(d). In actual practice, V_{xx} and V_{xy} were recorded as a function of I_{SD} and numerically differentiated with respect to I_{SD} with a finite difference of $\Delta I_{SD}\approx 0.1$ μA ($\Delta E\sim 1$ mV/cm). The accuracy of the data points of α and β in Figs. 4(c) and 4(d) is estimated to be better than $\pm 4\times 10^{-4}$. Values of α are positive since ψ increases with E, and β is positive because the increase in J with E is sublinear.

Knowing the values of $\alpha(E)$, $\beta(E)$, and $\psi(E)$, we can derive values of D, as plotted against E in Fig. 4(e) for elevated temperatures. While D exhibits general trend of increase with increasing E at all elevated temperatures, values of D for $T_L<28$ K are found to reach the threshold value, $D=0$. The critical values of $E=E_{NDC}$, at which $D=0$ is reached, are marked by the black dots in Fig. 4(e) and are listed in Table I for comparison with E_{th}. We note that the values of E_{NDC} agree extremely well with the values of $E=E_{th}$, at which the current instability is found to take place. (No adjustable parameters are used in the analysis.) We should also note that D for $T_L>30$ K do not reach $D=0$ in Fig. 4(e), which is consistent with the absence of current instability [Fig. 2(b)]. We hence conclude that the current instability found in the present experiments is caused by the NDC predicted by Kurosawa *et al.*[11]

We made similar analysis for $\nu=4$ and found similar nonlinearities, viz., α and β are positive and increase with increasing E; in addition, the absolute amplitudes of α and β are on the same order as those at $\nu=2$. Nevertheless, D stays within the negative (stable) region, not reaching zero at any temperatures studied. We identified that the difference arises from the smaller amplitude of the Hall angle, $\tan\psi=20\sim 30$, which is compared with the larger values, $\tan\psi=44\sim 93$ with $1.548<\psi<1.56$, at $\nu=2$.

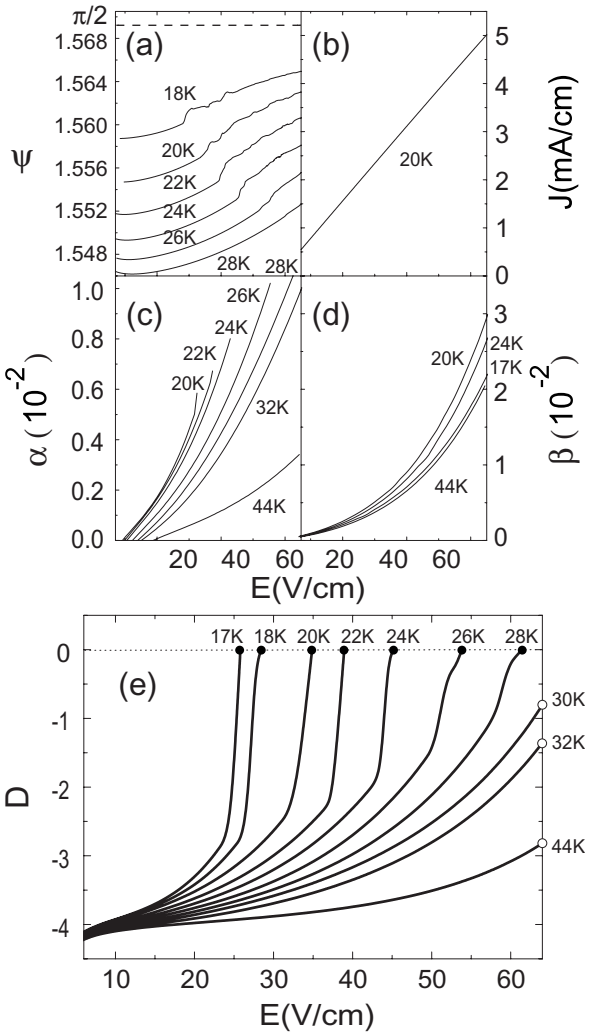

FIG. 4. (a) The Hall angle ψ and (b) the current density J against E at several elevated temperatures, as derived from the data of Fig. 3. ψ increases with E. The curves of J versus E obtained at $T_L=17\sim 44$ K are similar, and the increase in J is slightly sublinear. Nonlinear parameters (c) α and (d) β against E, deduced from the data shown in Figs. 4(a) and 4(b). (e) Values of D against E derived from the values of ψ, α, and β. Possible errors in the values of D and E are $\sim\pm 3.5\times 10^{-2}$ and $\sim 10^{-3}$ V/cm, respectively, which are small compared to the width of each line in the figure. The circles represent the terminal point of data analysis. The E-field values at which D equals 0 are denoted by E_{NDC} and marked by the black dots.

In sample 2, similar current instability is observed and ascribed to the NDC via similar analysis at $\nu=2$ ($B=7.8$ T) and $T_L=17\sim 35$ K. The current instability did not occur at $\nu=4$ ($B=3.9$ T). The overall feature of the nonlinearity is similar to that of sample 1, viz., V_{xx} sublinearly increases (R_{xx} decreases) with increasing I_{SD} up to $I_{SD}=I_{th}$; α is positive and increases with increasing E. In sample 2, however, R_{xy} slightly decreases with increasing I_{SD} and hence β is negative, which is a feature opposite to that of sample 1 [Fig. 3(b)]. Nevertheless, the effect of decreasing R_{xy} is quantitatively small and α remains to be positive.

When $\tan\psi\gg 1$, relation (2) can be well approximated by

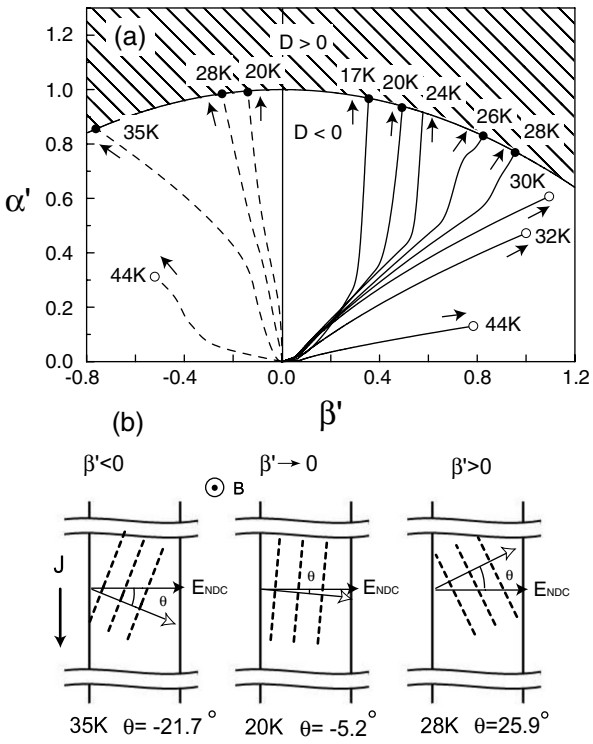

FIG. 5. (a) Stable and unstable regions in the α'-β' plane, separated by the parabola, $\alpha' = -\beta'^2/4 + 1$. Traces of α' and β' with increasing E are indicated by solid lines for sample 1 ($\beta' > 0$) and by dashed lines for sample 2 ($\beta' < 0$). Possible errors in the values of α' and β' are estimated to be $\sim \pm 2 \times 10^{-2}$. (b) The representative growth for each condition. The hollow arrow marks the direction of the eigenvector with the negative eigenvalue of σ^d. The dashed lines drawn perpendicular to the eigenvector represent the growth direction of charge filaments at $E = E_{\mathrm{NDC}}$.

$$\alpha' > -\beta'^2/4 + 1, \tag{3}$$

where $\alpha' = \alpha \tan \psi$ and $\beta' = \beta \tan \psi$ are parameters enhanced by $\tan \psi$. Figure 5(a) shows the parabola $\alpha' = -\beta'^2/4 + 1$ in the α'-β' plane, where the region of NDC regime is represented by shading. Relation (3) makes it explicit that large Hall angles ($\psi \sim \pi/2$) make NDC probable. That is, no matter how α and/or β are small, any system falls into NDC if $\tan \psi$ is sufficiently large. The data of sample 1 ($\beta > 0$, solid lines) and those of sample 2 ($\beta < 0$, broken lines) are shown together in Fig. 5(a). It is also revealed that in the present experiments α plays a primary role, while β (whether positive or negative) plays a secondary role of reducing E_{th}.

B. Space-charge domains

As mentioned in Sec. I (Fig. 1), charge domains are expected to develop in the regime of NDC. Reference 11 argued that the charge domains (needles) develop most rapidly in the direction perpendicular to the eigenvector associated with the negative eigenvalue of σ_S^d. Specifically, the eigenvector is at angle $\theta = (\psi + \varphi)/2 - \pi/4 \approx \varphi/2$ to E, where $\varphi \equiv \tan^{-1}(\beta'/\alpha') = \tan^{-1}(\beta/\alpha)$.[11] The probable direction of charge domains can thus be determined by the values of α' and β' at the terminal of each trace ($\alpha' = -\beta'^2/4 + 1$) in Fig. 5(a). In general terms, space-charge filaments are formed in the direction parallel to the current when $\beta' = 0$. When $\beta' < 0$ (> 0), the space-charge filaments tilt (anti) clockwise from J. Figure 5(b) schematically displays three examples chosen from the data of Fig. 5(a), viz., $\theta = -21.7°$ ($\beta' < 0$) for sample 2 at $T_L = 35$ K in the left, $\theta = -5.2°$ ($\beta' \sim 0$) for sample 1 at $T_L = 20$ K in the middle, and $\theta = 25.9°$ ($\beta' > 0$) for sample 1 at $T_L = 28$ K in the right. Further theoretical consideration suggests that the characteristic length scale of the period of the space-charge filaments is inversely proportional to the growth rate.[19]

Formation of space-charge filaments may be reminiscent of the current filaments formed in bulk systems of S-shaped J-E characteristics in the absence of magnetic field. It should be stressed, however, that in the entire range of study in the present experiments J-E relation remains to be single valued without exhibiting S-shaped or N-shaped relations. The current instability in the present experiments occurs without multivalued features of the J-E relation.

C. Low lattice temperatures

In the QH effect regime at low temperatures, the distribution of electric field or current density can be highly nonuniform, hindering quantitative analysis of nonlinear transport coefficients in the present studies. Nevertheless, the experimentally established fact that the QH effect is observable as a stable state is a proof that the linearity of the 2DEG system in the QH effect regime is so strictly satisfied that the NDC criterion [relations (2) or (3)] is not met anywhere in the conductor.[20]

At low T_L, the QH effect breaks down at higher currents ($I_{\mathrm{SD}} > 20$ μA). We find systematically different features in the breakdown regime between $\nu = 2$ and $\nu = 4$. At $\nu = 2$ the current becomes unstable in the breakdown regime but it remains stable at $\nu = 4$, namely, the current starts to fluctuate yielding irregular structures in the V_{xx} versus I_{DS} curve for $\nu = 2$ [at $T_L = 4.2$ and 7 K in Fig. 3(a)] but the current does not fluctuate and the curve of V_{xx} versus I_{DS} remains smooth without irregular structures for $\nu = 4$ [at 4.2 and 7 K in Fig. 2(b)]. Similar features were noted also in sample 2. The breakdown phenomenon has been interpreted as a transition of the electron system from the QH effect state with a low electron temperature, $T_e \sim T_L$, to a dissipative state with an elevated electron temperature, $T_e \sim \hbar\omega_c/(6k_B)$.[18] Noting that $T_e \sim \hbar\omega_c/(6k_B) \sim 16$ and 20 K ($\nu = 2$), respectively, in samples 1 and 2, we suppose that the electron system falls into the NDC regime when T_e is elevated by the QH effect breakdown for $\nu = 2$. In the condition of $\nu = 4$, however, the NDC criterion is not fulfilled even when T_e is elevated by the QH effect breakdown, similar to the case of elevated lattice temperatures at $\nu = 4$.

D. Mechanism of nonlinear response

NDC found in the present experiments is caused primarily by the increase in $\alpha = \partial\psi/\partial \log E$ [Fig. 5(a)] or a reduction in $\rho_{xx} = (V_{xx}/L)/(I_{\mathrm{SD}}/W)$ with increasing E [Fig. 3(a)]. This nonlinearity is likely to be a general trend followed by high-mobility 2DEG systems at high magnetic fields because it is

found as well in both samples 1 and 2 at $\nu=4$ and is reported also by other research groups.[13–16,21–23]

Reduction in ρ_{xx} at high magnetic fields ($\tan\psi \gg 1$) implies a decrease in the scattering rate. Simple electron heating effect is ruled out from relevant mechanisms because it would cause ρ_{xx} to increase. Indeed, Fig. 3(a) shows that ρ_{xx} increases with increasing T_L. Qualitatively, elastic Zener tunneling between Landau levels may be suppressed with increasing the electric field and ρ_{xx} might be thereby reduced.[23] It is unclear, however, if this effect gives quantitative account for the phenomenon found here.

In general nonlinear response arises via the effect of electric fields either on the kinematics of electron scattering[8,24] or on the electron distribution function.[25,26] Theory suggests that the later mechanism dominates in most experimental conditions, where the inelastic-scattering time $\tau_{\rm in}$ is much larger than the quantum or single-particle relaxation time τ_q, i.e., $\tau_{\rm in} \gg \tau_q$.[25] In strong magnetic fields $\omega_c\tau_{\rm tr} \gg 1$ ($\tau_{\rm tr}$ is the transport scattering time), random scattering process causes electrons to diffuse in the direction of electric field E. Since the electron energy changes by $eEdx$ after the diffusion at distance dx, the electron diffusion in space translates into the diffusion in energy, $\epsilon + eEdx$. It is theoretically shown, for high temperatures $k_BT_L > \hbar\omega_c$, that this leads to a nonequilibrium electron distribution function with an oscillatory structure of period $\hbar\omega_c$, where the distribution maxima do not coincide with the density of state maxima.[25] Since the oscillation amplitude increases with E, the average scattering rate decreases to reduce ρ_{xx}. In a simplified condition of overlapping Landau levels (relatively weak modulation in the density of states), analytical expression of the longitudinal conductivity σ_{xx} is given,[25] which is translated to

$$\frac{\rho_{xx}(E)}{\rho_{xx}(0)} = \left[1 + 2\delta^2\left(\frac{1-3Q_{\rm dc}}{1+Q_{\rm dc}}\right)\right]/(1+2\delta^2) \qquad (4)$$

through $\rho_{xx} \sim \rho_{xy}^2\sigma_{xx}$. Here, $\delta = \exp(-\pi/\omega_c\tau_q)$ is the Dingle factor with the quantum relaxation time τ_q at $E=0$. The electric field E is measured by

$$Q_{\rm dc} = \frac{2\tau_{\rm in}}{\tau_{\rm tr}}\left(\frac{eEv_F}{\omega_c}\right)^2\left(\frac{\pi}{\hbar\omega_c}\right)^2, \qquad (5)$$

where v_F is the Fermi velocity at $B=0$, and $\tau_{\rm tr}$ and $\tau_{\rm in}$ are the relevant scattering times at $E=0$.

Reference 13 reports that Eq. (4) accounts for the experimental results obtained in relatively small magnetic fields ($B<1$ T). Strictly the present experimental condition does not fit to the assumptions of $k_BT_L > \hbar\omega_c$ and the overlapping Landau levels. Nevertheless it may be interesting to compare Eq. (4) with our experimental results (sample 1 at $\nu=2$ and $B=5.88$ T). To quantify $\rho_{xx}(E)$ in Eq. (4), three parameters $\tau_{\rm tr}$, τ_q, and $\tau_{\rm in}$ have to be determined. As to the transport scattering time, $\tau_{\rm tr}=32$ ps at $T_L=4.2$ K is derived from $\mu = 8.0\times10^5$ cm^2/Vs. The values of $\tau_{\rm tr}$ at elevated temperatures are plotted against T_L in Fig. 6(b), where the values are deduced from the data in the limit of $I_{\rm SD}=0$ in Fig. 3(a) by assuming the Drude conductivity in strong B, $\sigma_{xx} = e^2N_0v_F^2/2\omega_c^2\tau_{\rm tr}$, with the density of states $N_0 = m^*/\pi\hbar^2$ at $B=0$. As to τ_q, Shubnikov–de Haas oscillations at T_L $=4.2$ K indicate $\tau_q=1.6$ ps ($T_L=4.2$ K).[27] We assume in turn that the ratio of $\tau_{\rm tr}/\tau_q \sim 20$ is independent of temperature, noting that the ratio can be treated as a material parameter.[28] Hence, we take $\tau_{\rm in}$ as the only one adjustable parameter.

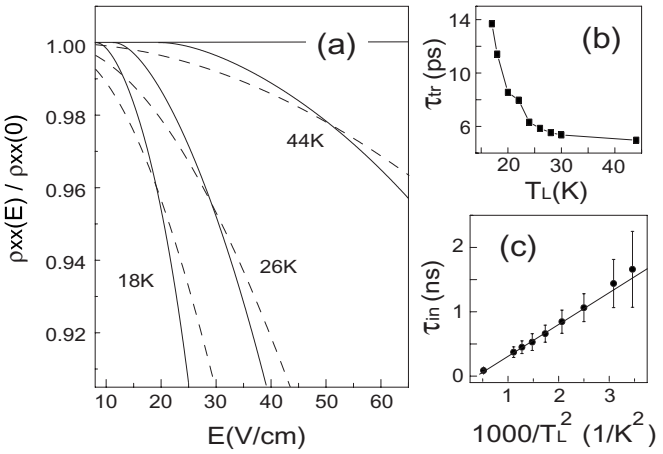

FIG. 6. (a) At $T_L=18$, 26, and 44 K, theoretical values of $\rho_{xx}(E)/\rho_{xx}(0)$ given in Eq. (4) (dashed lines) are compared with the experimental values (solid lines). (b) The transport scattering time $\tau_{\rm tr}$ versus temperature determined from the longitudinal resistivity at elevated temperatures. (c) The inelastic-scattering time, $\tau_{\rm in}$, determined in the fitting procedure in Fig. 6(a).

The solid lines in Fig. 6(a) are replots of the experimental data of Fig. 3(a) in terms of the normalized $\rho_{xx}(E)$ at several elevated temperatures. The experimental curves are fairly well reproduced by the dashed lines drawn according to the theoretical values of Eq. (4). The parameter values, $\tau_{\rm in}$, used for the best fit at different temperatures are plotted in Fig. 6(c). The relation, $\tau_{\rm in} \propto 1/T_L^2$, is noted, which agrees with theoretical expectation. Absolute values $\tau_{\rm in}=487/T_L^2$ (ns) are much larger than those $\tau_{\rm in}=10\sim12/T_L^2$ (ns) reported for $B=0.9425$ T in Ref. 13. If the difference can be ascribed to the difference in magnetic field amplitude, $\tau_{\rm in} \propto B^{2.1}$ is suggested.

We should remember also that the validity of the present analysis is limited. Especially, more realistic density of states, consisting of well-separated discrete Landau levels, should be taken into account for more detailed quantitative discussion.

IV. CONCLUSIONS

In summary we have found that 2DEG systems at $\nu=2$ quantum-Hall plateau exhibit current instability at $T_L \sim 17-35$ K, viz., the longitudinal voltage begins to fluctuate when the current passing through Hall-bar samples exceeds a threshold value. Through the analysis of experimental results we have proven that the instability is caused by the NDC predicted by Kurosawa *et al.* in Ref. 11. Unlike the NDC at $B=0$, the NDC found in 2DEG systems in high magnetic fields occurs in a single valued J-E relation. Reduction in the longitudinal resistivity with increasing the current, which is a general trend of high-mobility 2DEG systems at strong magnetic fields, is the driving force of the NDC. The physical

origin of the longitudinal resistivity reduction is suggested to be related to an electric-field-induced nontrivial electron distribution function.

ACKNOWLEDGMENTS

We acknowledge Chung-Yu Mou, Daw-Wei Wang, C. C. Chi, and Chi-Shung Tang for helpful discussions and Kuan-Ting Lin for the experimental assistance. J. C. Chen thanks the National Center for Theoretical Sciences in Taiwan for numerous help. This work was supported by the National Science Council of Taiwan (Grant No. NSC 95-2112-M-007-049-MY3), the TOP project of the university, and by a Grant-in-Aid for Scientific Research (A) (Grant No. 19204031) from the Japan Society for the Promotion of Science.

[1] R. G. Mani, J. H. Smet, K. von Klitzing, V. Narayanamurti, W. B. Johnson, and V. Umansky, Nature (London) **420**, 646 (2002).
[2] M. A. Zudov, R. R. Du, L. N. Pfeiffer, and K. W. West, Phys. Rev. Lett. **90**, 046807 (2003).
[3] M. A. Zudov, R. R. Du, J. A. Simmons, and J. R. Reno, Phys. Rev. B **64**, 201311(R) (2001).
[4] A. V. Andreev, I. L. Aleiner, and A. J. Millis, Phys. Rev. Lett. **91**, 056803 (2003).
[5] P. W. Anderson and W. F. Brinkman, arXiv:cond-mat/0302129 (unpublished).
[6] F. S. Bergeret, B. Huckestein, and A. F. Volkov, Phys. Rev. B **67**, 241303(R) (2003).
[7] J. Shi and X. C. Xie, Phys. Rev. Lett. **91**, 086801 (2003).
[8] A. C. Durst, S. Sachdev, N. Read, and S. M. Girvin, Phys. Rev. Lett. **91**, 086803 (2003).
[9] A. F. Volkov and S. M. Kogan, Sov. Phys. Usp. **11**, 881 (1969).
[10] S. M. Kogan, Sov. Phys. Solid State **10**, 1213 (1969).
[11] T. Kurosawa, H. Maeda, and H. Sugimoto, J. Phys. Soc. Jpn. **36**, 491 (1974).
[12] T. Takamasu, S. Komiyama, S. Hiyamizu, and S. Sasa, Proceedings of the 18th International Conference on the Physics of Semiconductors, edited by O. Engström (World Scientific, Singapore, 1986), p. 433.
[13] J.-q. Zhang, S. Vitkalov, A. A. Bykov, A. K. Kalagin, and A. K. Bakarov, Phys. Rev. B **75**, 081305(R) (2007).
[14] W. Zhang, H.-S. Chiang, M. A. Zudov, L. N. Pfeiffer, and K. W. West, Phys. Rev. B **75**, 041304(R) (2007).
[15] A. A. Bykov, J.-q. Zhang, S. Vitkalov, A. K. Kalagin, and A. K. Bakarov, Phys. Rev. Lett. **99**, 116801 (2007).
[16] W. Zhang, M. A. Zudov, L. N. Pfeiffer, and K. W. West, Phys. Rev. Lett. **100**, 036805 (2008).
[17] M. E. Cage, R. F. Dziuba, B. F. Field, E. R. Williams, S. M. Girvin, A. C. Gossard, D. C. Tsui, and R. J. Wagner, Phys. Rev. Lett. **51**, 1374 (1983).
[18] S. Komiyama and Y. Kawaguchi, Phys. Rev. B **61**, 2014 (2000).
[19] T. Kurosawa and S. Nagahashi, J. Phys. Soc. Jpn. **45**, 707 (1978).
[20] To be more explicit, additional measurements show that $\tan\psi > 10^7$ at $T_L < 4.2$ K for $\nu=2$, which implies that the nonlinear parameters are small such that $\alpha, |\beta| < 10^{-7}$.
[21] S. Komiyama, T. Takamasu, S. Hiyamizu, and S. Sasa, Solid State Commun. **54**, 479 (1985).
[22] T. Takamasu, S. Komiyama, S. Hiyamizu, and S. Sasa, Surf. Sci. **170**, 202 (1986).
[23] C. L. Yang, J. Zhang, R. R. Du, J. A. Simmons, and J. L. Reno, Phys. Rev. Lett. **89**, 076801 (2002).
[24] M. G. Vavilov and I. L. Aleiner, Phys. Rev. B **69**, 035303 (2004).
[25] I. A. Dmitriev, M. G. Vavilov, I. L. Aleiner, A. D. Mirlin, and D. G. Polyakov, Phys. Rev. B **71**, 115316 (2005).
[26] M. G. Vavilov, I. L. Aleiner, and L. I. Glazman, Phys. Rev. B **76**, 115331 (2007).
[27] T. Ando, A. B. Fowler, and F. Stern, Rev. Mod. Phys. **54**, 437 (1982).
[28] S. Das Sarma and F. Stern, Phys. Rev. B **32**, 8442 (1985).